NUMERICAL AND EXPERIMENTAL STUDY OF ABSORPTION OF H_2O VAPOR IN WAVY FALLING FILM OF LiBr AQUEOUS SOLUTION IN VERTICAL TUBES AND IN PRESENCE OF NON-ABSORBABLES

E. Garcia-Rivera[a], J. Castro[a], J. Farnós[a], C. Oliet[a]

[a] *Centre Tecnològic de Transferéncia de Calor (CTTC), Universitat Politécnica de Catalunya (UPC), ETSEIAT, Colom 11, E08222 Terrassa (Barcelona), Spain*

Abstract

One of the main reasons for the discrepancies between theoretical predictions of absorption phenomena made by mathematical models when they are compared against experimental results under real conditions, are the presence of non-absorbable gases. It is well known that these non-absorbable gases inside the shell of the absorption chiller are produced mainly for two reasons: i) air leakages (Oxygen-Nitrogen); ii) gases produced by corrosion (Hydrogen). In order to evaluate the influence of the presence of non-absorbable gases, an experimental set-up which reproduces vapor absorption in a vertical falling film has been designed and built with a mass spectrometer analyzer. Parallelly, a mathematical model of falling film absorption of H2O by LiBr aqueous solution that considers the influence of non-absorbable gases has been implemented. The model is semi-empirical, based on Navier Stokes equations together with energy and mass species simplified under the boundary layer hypotheses. Several experimental tests have been performed to determine the influence of the air concentration in the absorption performance. Moreover, a comparison of numerical results against experimental data has been performed under different working conditions with reasonable agreement.

Keywords:
absorption, LiBr, wavy falling film, numerical, experimental, non-absorbables

1. Introduction

The air intrusions into absorption machines are the main cause of the unacceptable galvanic corrosion due to the reaction of the entered Oxygen (O_2) with the metallic parts. When non-absorbable gases are present, they tend to get swept toward the vapor-liquid interface by the process of absorption of the vapor, and it causes maximum air concentration at the interface. Therefore, absorption pressure is reduced to partial water vapor pressure in the interface which significantly reduces the rate of absorption.

The influence of non-absorbable has been studied experimentally by several authors. Kim et al. (1995) used the "freezing out method"technique to evaluate the quantity of non-absorbable gases, and they estimate its value at the interface indirectly. The "freezing out methodçonsists of a sampler container in which the temperature and pressure were measured before and after that the enclosed water vapor was condensed. The authors presented the experimental results of the influence of the inlet solution temperature in the form of Sherwood vs. the values of the logarithmic mean concentration difference. They concluded that the Sherwood number decreases about 20 % when air content increases from 0,5 to 15 %.

Kim et al. (1996) reported both the "freezing out method.ªnd the mass spectrometer gas analyzer as measurement techniques in order to measure the air concentrations, but only the first method was reported as used. The authors conclude that the mass transfer is decreased up 20 % with air concentration increases from 0,5 to 14 %.

Ameel et al. (1996) reported experimental results of absorption of water vapor in a vertical liquid film in a solar cooling system. They also used the "freezing out method"to measure the air percentage in the vapor phase which varies from 0 to 7 % with a maximum decrement in the mass transfer rate of about 35 % approximately. Kim and Lee (2003) performed an experimental study for horizontal falling film absorbers. The authors reported a variation of non-absorbable gases from 0,17 % to 10 %. They conclude that the presence of about 2 % volumetric concentration of air resulted in a 25 % reduction in the Nusselt number, and 41 % reduction in the Sherwood number. As the previously referred authors, they also use the "freezing out method"to evaluate the quantity of non-absorbable gases. Yang (1987) in his dissertation performed a study of the influence of non-absorbable gases using a mass spectrometry technique. He reported air concentrations from about 4 % until 30 %. He observed heat and mass transfer reductions about 50 % and 75 %.

The Table 1 shows a summary of the experimental investigation of non-absorbable gases for different authors.

w_{air} %	Percentages of rate absorption reduction (R %)				
	Kim J. K. (1995)	Kim J. K. (1996) $\star$	Ameel $\star$	Kim B. $\star$ $*$	Yang $\star$
0.17				10	
2.0				25	
4.0					50
7.0			35		
10.0					
15.0	20	20			
30.0					75

Cuadro 1: Comparison of percentages of rate absorption reduction (R) at different air concentrations for different authors (experimental research). The symbol $\star$ refers to freezing out method and $*$ refers to mass spectrometry analysis.

On the other hand, the influence of non-absorbable has been also studied numerically. Sabir et al. (1995) developed a mathematical model based on energy and mass balances. They also reported that the presence of only 2 % of air causes a reduction of more than six times on the overall effectiveness. Ameel et al. (1996) presented analytical methods to estimate the reduction in the absorption phenomena, but it is restricted only in the entrance region of the falling film, where an analytical solution to the governing equations is possible. The authors reports that 10 % of air reduces about 26 % the heat and mass transfer rates. Yang and Chen (1991) developed a mathematical model for smooth falling film absorption. These authors used a set of partial differential equations in its parabolic form and considering only velocity components in the x-direction. Such equations are applied in both liquid film and vapor side. They reported that a value of 0.01 % reduces drastically (about 84,96 %) the rates of heat and mass transfer. Yang and Wood (1991) developed a mathematical model for wavy flow in vertical film absorption. In spite of their results show an improvement respect to the smooth falling film model, the predicted effects of non-absorbable gases in absorption performance were still severe. The authors reported that a value of only 0,01 % reduces 65 % the rates of heat and mass transfer. In a latter work, Yang and Jou (1998), the authors improve their predictions of the mass transfer rates. However, their model overpredicts mass transfer rates at low non-absorbables concentrations and still underpredicts mass tranfer rates at high non-absorbables

concentrations.

Medrano et al. (2003) proposed a one-dimensional empirical model based on three ordinary differential equations. The authors also considered the bulk outlet air concentration, which is calculated based on an air mass balance in the absorber. The outlet air concentration is function of the theoretical purge velocity. In this way, the authors are able to evaluate the influence of the purge velocity during the absorber performance in presence of non-absorbable gases. They reported a 61 % reduction in mass absorption flux when there was an 20 % of air concentration and the maximum purge velocity (30 $m \cdot s^{-1}$). However, in absence of purge velocity, the reduction in mass absorption flux is about 90 % at the same conditions. Grossman and Gommed (1997) developed a mathematical model based on the energy and mass species equations that are solved analytically in the entrance region in both the liquid and gas phases. The authors found that values of 0,1 % of air concentration results in 73 % of the reduction in the absorption rates. This author performed a previous attempt of a mathematical model García-Rivera et al. (2012) of falling film absorption of H_2O vapor by $LiBr$ aqueous solution with non-absorbable gases. The model was based on Navier-Stokes equations together with energy and mass species simplified under the boundary layer hypotheses in the liquid side. In order to calculate gradient of air at the interface, the penetration theory was applied in order to avoid a detailed calculation of the gas phase. It was detected that a value of only 0,01 % of air concentration results in 93,5 % of reduction in absorption rate. The Table 2 shows a summary of the results of the numerical investigations for different authors.

Along this paper is presented a mathematical model that predicts the effects of non-absorbable gases on the performance of a vertical absorber. The model is divided in three parts: i) coolant; ii) solid; iii) falling film. In the coolant the governing conservation equations (mass, momentum and energy) are solved by means of a step-by-step procedure. The heat conduction equation is solved for the solid. In the falling film the model, is semi-empirical, based on Navier-Stokes equations together with energy and mass species simplified making an order of magnitude analysis. The coupled equations are solved using finite difference method, and they are solved in both the liquid and gas phases. A detailed treatment of the liquid-vapor interface boundary conditions for the $LiBr$ and H_2O has been implemented (energy and mass balances). The diffusion coefficient for the vapor side was taken from Bird et al. (1960); Bennett and Myers (1975); Welty et al. (2008).

w_{air} %	Percentages of rate absorption reduction (R %)							
	Sabir	Ameel	Yang & Chen	Yang & Wood	Yang & Jou	Medrano	Grossman	García
0.01			84.96	65				
0.1							73	93.5
1.0			85.32			18.18	90	93.74
2.0	48							
5.0			85.76		38	63.63	96.6	94.51
8.0		20						
10.0		26	86.37		40	81.81		95.37
15.0	53							
20.0						94.44	98.67	
30.0			88.75		44			99.64
48.0	69							
85.0	80							

Cuadro 2: Comparison of percentages of rate absorption reduction (R) at different air concentrations for different authors (numerical research).

2. Experimental Setup

The experimental setup and its main components are shown in Fig.1. The container (V1) is situated at the top of the structure. It has a capacity of approximately 17 litres (V1). It works as a generator, and it uses both an immersion heater of 2 kW and a set of flexible silicone rubber heaters placed directly on the outer surface with a total heating capacity of 4.4 kW. Each one of the heat generation sources is governed by an independent PID control. The absorber (A) is a single vertical tube (stainless steel), with a 0.022 m outer diameter and 0.018 m inner diameter. In order to visualize the absorption process, the vertical absorber is situated inside a borosilicate glass cover with a 0.315 m diameter and 1.5 m length. Two metal plates coupled with flat O-rings of NBR are situated both at the top and bottom of the glass container. The vertical absorber tube passes through the upper metal plates. The measuring instruments used are as follows: Resistance Temperature Detectors (RTD), Coriolis mass flow-meters and densimeters (C1, C2, C3) and pressure sensors (PS1, PS2). Other components are: gear pumps (P1, P2, P3, P7), peristaltic pump (P6), vacuum pumps (P4,P5), thermal baths (TB1, TB2), plate heat exchanger (HX). There are three different circuits in the experimental apparatus: (i) $LiBr$ aqueous solution, (ii) H_2O vapour and (iii) H_2O coolant. The circuit (i) begins in (V1) where the $LiBr$ aqueous solution is heated, and water vapour is generated. The temperature in (V1)

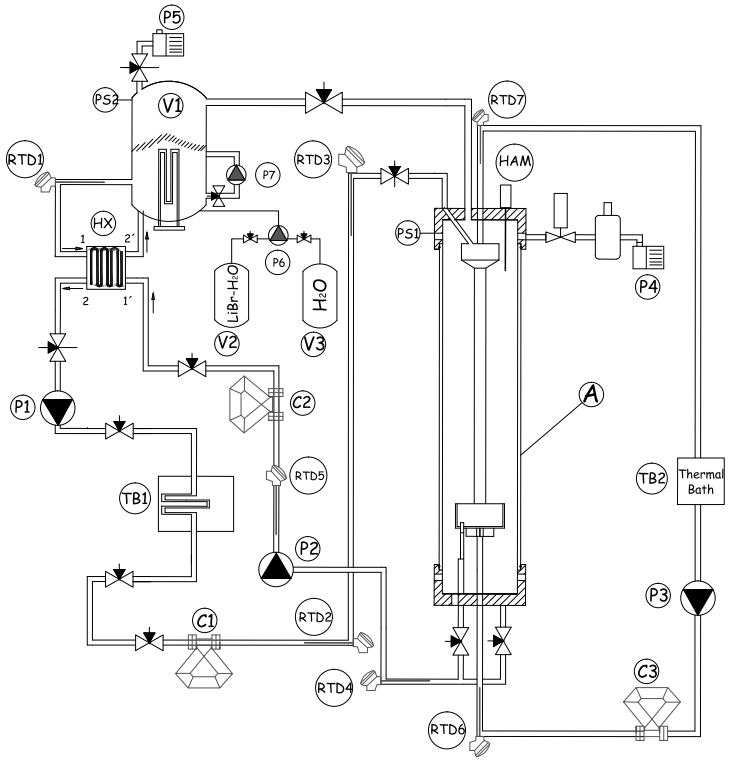

Figura 1: Falling Film Experimental Apparatus.

is controlled by (RTD1). The rich solution is pumped from the generator and it passes across a heat exchanger (HX), where points 1 and 2 represent the inlet and the outlet of the plate heat exchanger.

The inlet mass flow and density are measured by (C1), the rich solution enters at the top of the absorber where it is collected in the dispenser which creates the falling film on the outer side of the vertical tube. While the fluid is flowing down, the absorption is produced. The bottom dispenser picks up the weak solution which is sent back to the generator using the gear pump (P2). Both mass flow and density of the outlet solution are measured by (C2). The solution passes across (HX), where points $1'$ and $2'$ represent the inlet and the outlet of the plate heat exchanger respectively. The water vapour flows from the top of the generator to the absorber. During the generation process, the pump (P7) recirculates the aqueous solution. This is useful in

order to maintain a homogeneous temperature inside the generator. Both absorption and generation pressures are measured using the pressure gauges (PS1) and (PS2), respectively. Since concentration is an important factor, it is necessary to adjust it in a accurate way. A peristaltic pump (P6), together with vessels (V2) and (V3), are used to establish concentration. (V3) contains H_2O, while (V2) contains highly concentratred $H_2O - LiBr$ solution. Using the pump (P6) it is possible to increase or decrease the concentration in the generator by adding either H_2O or $H_2O - LiBr$ solution. Both concentration of the rich and the poor solution can be calculated since $c = f(\rho, T)$. Thus, (RTD2) and (RTD5) are used for obtaining concentrations while (RTD3) and (RTD4) are used for calculating an energy balance in the absorber. The coolant circuit is fed directly by the thermal bath (TB2), where the inlet temperature can be adjusted, and the coolant fluid is pumped in counter-flow. On the other hand, an energy balance in the coolant fluid is performed using (RTD6) and (RTD7). The thermal bath (TB1) is used to adjust the inlet temperature of the rich solution. During absorption process, this is a key issue to maintain this temperature under control due to its influence in the absorption process. Finally, the vacuum pumps (P4) and (P5), together with a liquid nitrogen cold trap, are used for removing non-absorbable gases. In order to avoid problems of condensations with RTD measurements for the vapour temperature, the authors have used an thermistor coupled with the optical sensor (HAM) in order to obtain more accurate measurements.

A mass spectrometry technology for Residual Gas Analysis (RGA) has been used to measure the presence of non-absorbable gases. The RGA technology provide an adequate technique into the vacuum environment for contamination monitoring, leak detection and analysis of the species of interest within the vacuum chamber.

In order to verify the reliability of the mass spectrometry data a second sensor was used. An optical sensor for dissolved oxygen was used for this purpose. Thus the O_2 percentage can be evaluated by two different methods with a reasonable agreement.

3. Mathematical model

The mathematical model is an extension of the one presented by García-Rivera et al. (2016). In the falling film flow, the same set of equations is discretized in both domains, liquid and vapor. In order to develop a model with relatively low computational cost, the wavy regime is introduced by

solving the Free Surface Deflection Equation, Yang (1987); Yang and Wood (1991); Yang and Jou (1993); Hirshburg (1980); Hirshburg and Florschuetz (1982a,b). The Fig. 2 shows details of the vertical falling film and its boundary conditions.

The following hypotheses are assumed:

I Steady state flow.

II Physical properties are variable only in flow direction.

III There is no shear stress at the interface.

IV Thermodynamic equilibrium at the interface.

V The flow is laminar or wavy laminar and incompressible.

VI The diffusion terms are negligible in the flow direction.

VII The convection terms are negligible in the direction orthogonal to the flow.

VIII The pressure gradients are negligible.

IX The initial velocity in liquid side considered corresponds to fully developed flow.

X The initial velocity in vapor side corresponds a parabolic profile that is function of interfacial velocity.

XI Dufour and Soret effects have not been considered.

XII The domain vapor side behaves like a boundary layer.

XIII The concentration of air at the liquid-vapor interface is dependent of the stream wise coordinate.

XIV Curvature effects due to wavy flow are neglected, as it is supposed the lenght of the waves much higher than film thickness. Therefore, flow separation effects are not considered Dietze (2010)

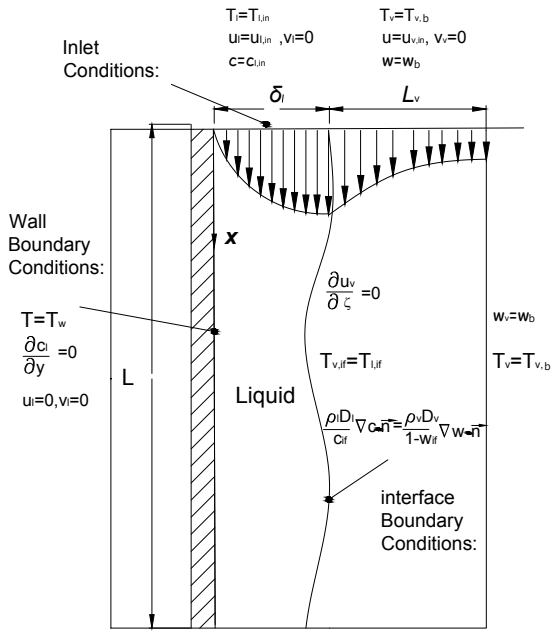

Figura 2: Schematic representation of the vertical falling film absorption in presence of non-absorbable gases.

According to the above mentioned hypotheses, the governing conservation equations of mass (1), momentum (2), energy (3) and mass species (4) can be written as:

$$\frac{\partial u_l}{\partial x} + \frac{\partial v_l}{\partial y} = 0 \tag{1}$$

$$u_l \frac{\partial u_l}{\partial x} + v_l \frac{\partial v_l}{\partial y} = g cos(\theta) + \nu_l \frac{\partial^2 u_l}{\partial y^2} \tag{2}$$

$$u_l \frac{\partial T_l}{\partial x} + v_l \frac{\partial T_l}{\partial y} = a_l \frac{\partial^2 T_l}{\partial y^2} \tag{3}$$

$$u_l \frac{\partial c}{\partial x} + v_l \frac{\partial c}{\partial y} = D_l \frac{\partial^2 c}{\partial y^2} \tag{4}$$

And the boundary conditions,

$$x = 0 \begin{cases} T_l = T_{l,in} & (a) \\ c = c_{in} & (b) \\ u_l = u_{l,in} & (c) \\ v_l = 0 & (d) \end{cases} \tag{5}$$

$$y = 0 \begin{cases} T = T_w & (a) \\ \nabla c \cdot \vec{n} = 0 & (b) \\ u = 0 & (c) \\ v = 0 & (d) \end{cases} \tag{6}$$

$$y = \delta_l \begin{cases} T_{l,if} = f(P_{H_2O,if}, c_{if}) & (a) \\ -\lambda_l \nabla T_l \cdot \vec{n} = h_{abs} \dot{m}_{abs_v} - \lambda_v \nabla T_v \cdot \vec{n} & (b) \\ \frac{\partial u_l}{\partial \zeta} = 0 (c) \end{cases} \tag{7}$$

The governing equations in vapor side are:

$$\frac{\partial u_v}{\partial x} + \frac{\partial v_v}{\partial y} = 0 \tag{8}$$

$$u_v \frac{\partial u_v}{\partial x} + v_v \frac{\partial v_v}{\partial y} = gcos(\theta) + \nu_v \frac{\partial^2 u_v}{\partial y^2} \tag{9}$$

$$u_v \frac{\partial T_v}{\partial x} + v_v \frac{\partial T_v}{\partial y} = a_v \frac{\partial^2 T_v}{\partial y^2} \tag{10}$$

$$u_v \frac{\partial w}{\partial x} + v_v \frac{\partial w}{\partial y} = D_v \frac{\partial^2 w}{\partial y^2} \tag{11}$$

and the corresponding boundary conditions,

$$x = 0 \begin{cases} T_v = T_{v,b} & (a) \\ w = w_b & (b) \\ u_v = u_{v,in} & (c) \\ v_v = 0 & (d) \end{cases} \tag{12}$$

$$y = \delta_l \begin{cases} T_{v,if} = T_{l,if} & (a) \\ -\frac{\rho_l D_l}{c_{if}} \nabla c \cdot \vec{n} = -\frac{\rho_v D_v}{(1-w_{if})} \nabla w \cdot \vec{n} & (b) \\ u_{v,if} = u_{l,if} & (c) \\ v_{v,if} = v_{l,if} & (d) \end{cases} \tag{13}$$

$$y = \delta_l + \delta_v \begin{cases} T_v = T_{v,b} & (a) \\ w = w_b & (b) \\ \frac{\partial u_v}{\partial \zeta} = 0 & (c) \end{cases} \tag{14}$$

The conservation equations for the liquid and vapor phases are respectively: mass (1) and (8), momentum (2) and (9) , energy (3) and (10) and mass species (4) and (11). The equations system in partial differential is solved by means of a change of coordinates taking into account the variation of the thickness of the falling film in the case of the liquid film thus, $\zeta_l = \frac{y_l}{\delta_l}$, and using an appropriate thickness (L_v) in the vapor side domain, thus $\zeta_v = \frac{L_v}{\delta_v}$.

In order to determine the domain on the vapor side, an evaluation of the Pr_v and Sc_v numbers was performed. The following expression is used in order to evaluate the relation between the boundary layers (momentum, thermal and concentration) Welty et al. (2008),

$$\frac{\delta_v}{\delta_{v,con}} = Sc_v^{1/3} \tag{15}$$

$$\frac{\delta_v}{\delta_{v,temp}} = Pr_v^{1/3} \tag{16}$$

In the case of vapor phase, $Pr_v > 1$ and $Sc_v < 1$, then $\delta_{v,temp} < \delta_v$ and $\delta_{v,con} > \delta_v$. Therefore the domain length in the vapor side should be $L_v \geq \delta_{v,con}$.

If performing a magnitud order evaluation Peclet number results in $Pe_l \sim 10^5$ and $Pe_v \sim 10^2$. When the Peclet number is zero, pure diffusion transport

is present, but it becomes negligigle compared with convective transport when Peclet number are higher than 2.

The equations (5 a-d) represent the inlet conditions, the inlet solution temperature ($T_{l,in}$) and the inlet mass concentration ($c_{l,in}$) that are known data. The inlet velocity solution ($u_{l,in}$) is calculated by means of the Nusselt's typical velocity profile. The equations (6 a-d) represent the wall boundary conditions, where T_w is the wall temperature, and $\nabla c \cdot \vec{n} = 0$ depicts impermeable wall condition. The equations (7 a-c) describe the conditions of the interface. The equation (7 a) refers to the equilibrium condition in liquid-vapor interface. Notice that the term $P_{H_2O,if}$ varies its value along the stream-wise direction, (7 b) represents the energy balance in the interface and the equation (7 c) means no shear stress at the interface. The kinematic conditions is satisfied by means of the mass conservation equation at the interface. Equations (12 a-d), represents the inlet conditions the vapor side for the temperature, concentrations, and velocity components, respectively; the equation (13 a) represents the temperature of the vapor in the interface that is equal to temperature of liquid in the interface; the equation (13 b) represents the water vapor absorbed through the interface, expressed by means the Fick's law in both liquid and vapor sides, the equation (13 c) represents that the component of the velocity in normal direction to the interface is the same for both liquid and vapour; the equation (14 a) refers to vapor temperature in bulk, the equation (14 a-c) refers to the boundary conditions of the limit of the potential zone in the vapor: temperature and water vapor concentration are known, and null derivative of the velocity normal to boundary layer in vapor side.

In order to close the mathematical models presented previously, some extra relations are needed. The Fig. 3 depicts the mass concentration gradients in both liquid and vapor phases. When the absorption is produced, the non-absorbable gasses tend to migrate to the interface due to the motion of the vapor absorbed. However, because the gas is not absorbed, it accumulates at the vapor-liquid interface. The expression which relates the mass concentration with the partial pressure in the vapor phase are given by:

$$w_b = \frac{P_{H_2O,b} N_{H_2O}}{P_{H_2O,b} N_{H_2O} + P_{air,b} N_{air}} \tag{17}$$

$$w_{if} = \frac{P_{H_2O,if} N_{H_2O}}{P_{H_2O,if} N_{H_2O} + P_{air,if} N_{air}} \tag{18}$$

$$P_t = P_{H_2O,b} + P_{air,b} \tag{19}$$

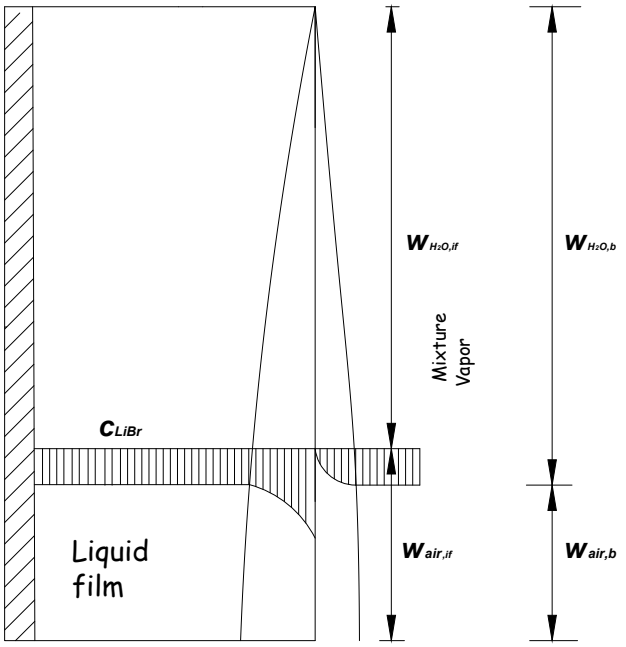

Figura 3: Mass concentrations gradients in vapor side along a vertical falling film (bulk and interface)

The set of conservation equations for liquid are (1)-(4), for vapor (8)-(11) and the relations (17)-(19) and the appropriate boundary conditions (5)-(7) and (12)-(14) are solved by means the algorithm described in next section.

4. Resolution procedure

Three different domains are used in the calculation: i) $LiBrH_2O$ liquid falling film solution, ii) coolant fluid domain, and iii) wall tube (solid). Each domain is discretized and solved independently. For the coolant fluid domain (ii) and the solid one (iii), the mesh is coincident in vertical direction, but in radial direction, only one control volume is needed for each the domains. On the other hand, for the falling film solution domain, an extra mesh intensification is needed in vertical direction, and, moreover, meshing is needed

in radial direction too. In both fluid domains (i) and (ii) the interchange of information goes through the solid domain (iii). The complete resolution is achieved when temperature field in wall tube do not undergoes changes in its value between consecutive iterations.

4.1. Falling Film Domain

The resolution algorithm for the falling film absorption model based on boundary layer hypotheses in the presence of non-absorbable gasses is described below.

1. Coupled resolution of mass (1) and momentum (2) conservation equations, for obtaining the values of the components of the velocity. Calculation of the boundary layer thickness considering a smooth film thickness.

2. The Free Surface Deflection Equation is solved to obtain wave profile which is function Re and dimensionless surface tension parameter . The new boundary layer thickness as function of wave profile is calculated and introduced. See García-Rivera et al. (2016) for further details.

3. Calculation of $c_{l,if}$ based on a mass balance, the equation (13 b) and using secant method.

4. Calculation of w_{if} based on a energy balance, the equation (13 b) and using secant method.

5. Calculation of temperatures fields, T_l and T_v, using equations (3) and (10) respectively. The equilibrium condition in the interface is imposed by $T_l = T_v = f(c_{if}, P_{H_2O,if,v})$. Calculation of concentration field in the vapor side w using equation (11).

6. Calculation of the mass absorbed from the point of view of the vapor side ($\dot{m}_{abs}$ right side of equation 13 b), calculation of the energy balance at the interface using equation (7 b).

7. Check if energy balance is accomplished, equation (7 b). If so, go to the next step, if not, back to the point 4.

8. Calculation of the concentration field in liquid side c_l using the equation (4).

9. Calculation of the mass absorbed from the point of view of the liquid side, ($\dot{m}_{abs,l}$ left side of equation (13b)), calculation the energy balance at the interface using equation (7 b).

10. Check if mass balance in the interface is accomplished, (see equation 13 b),
$\left|\frac{\rho_l D_l}{c_{if}}\nabla c\cdot\vec{n}-\frac{\rho_v D_v}{(1-w_{if})}\nabla w\cdot\vec{n}\right|<\varepsilon$. If so, go to the next step, if not back to the point 3.

11. Check if mass absorbed between two consecutive iterations has not variation $|\frac{\dot{m}_{abs}-\dot{m}_{abs_o}}{\dot{m}_{abs}}|\leq\varepsilon$. If so, go to the next row, if not back to the point 1.

4.2. Coolant Domain

The coolant water in counter flow is solved numerically using the equations of conservation of mass, momentum and energy in its integral form. A step-by-step procedure similar to Ablanque et al. (2015) has been implemented, simplified to single phase flow.

1. Calculation of fluid properties ($\rho, \mu, h\ldots$) in function of T_c and P_c.

2. Resolution of mass conservation equation.

3. Resolution of momentum conservation equation in order to obtain P_i, factor friction is obtained from Ravigururajan and Bergles (1996).

4. Resolution of energy conservation equation in order to obtain T_i, the heat transfer coefficients are obtained from Gnielinski (1976).

5. Check if mass and energy balances are accomplished. If so, go to the next control volume, if not, back to the point 2.

4.3. Solid Domain

Solid domain is solved by applying the energy equation in its integral form.

1. Solve energy conservation equation in order to obtain field temperature along the wall tube Tw ($\forall$ i).

2. Evaluate $|\frac{T_w-T_w^o}{T_w}|\leq\varepsilon$. If the previous condition is not fulfilled back to calculating falling film domain.

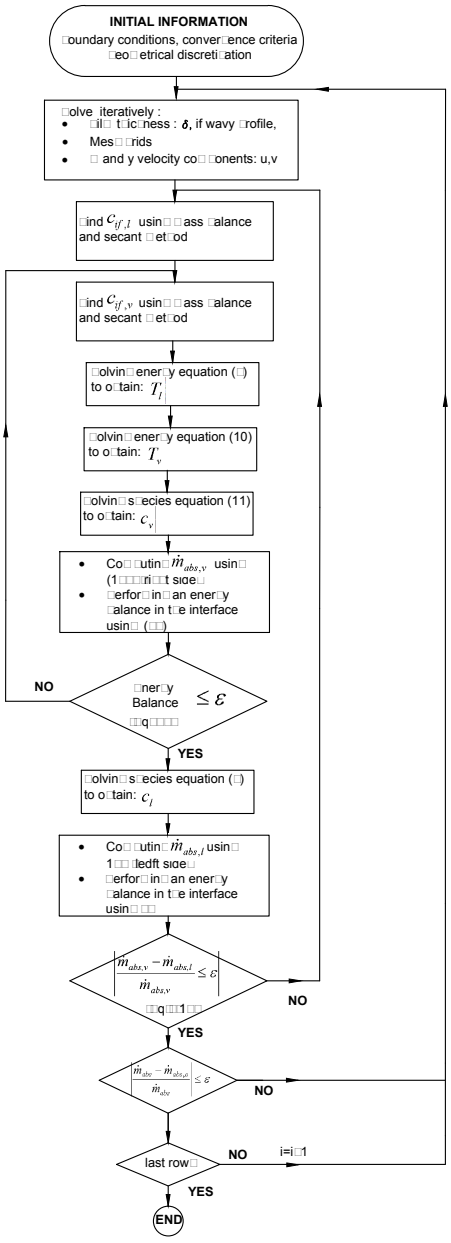

Figura 4: Resolution algorithm for boundary layer mathematical model falling film absorption in presence of non absorbable gases.

4.4. Calculation of Mass Diffusivity in the Water-Vapor Mixture

Unlike the two other molecular transport coefficients for gases, the viscosity and thermal conductivity, the gas-phase diffusion coefficient is strongly dependent on the pressure and the temperature. Specifically, the gas-phase diffusion coefficient is an inverse function of total system pressure $D_v \propto \frac{1}{P_v}$ and a $\frac{3}{2}$ power-law function of the absolute temperature $D_v \propto T_v^{\frac{3}{2}}$. Since the working pressures in $LiBr$ absorbers are relative low, it is expected that D_v values were higher in $H_2O-LiBr$ solution than in atmospheric pressure. The diffusion coefficient of the mixture water vapor-air is obtained from Welty et al. (2008) and Bennett and Myers (1975), using the expression proposed by Hireschfelder,

$$D_v = \frac{0{,}001858 T_v^{\frac{3}{2}} \left[\frac{1}{N_{air}} + \frac{1}{N_{H_2O}}\right]^{1/2}}{Pr_{AB}^2 \Omega_D} \tag{20}$$

The above equation is used for adjusting experimental data and for moderate ranges of pressure, up to 25 atm. For lower pressures the following expression is used:

$$D_{v,T_2,P_2} = D_{v,T_1,P_1} \left(\frac{P_1}{P_2}\right) \left(\frac{T_1}{T_2}\right)^{\frac{3}{2}} \frac{\Omega_{D|T_1}}{\Omega_{D|T_2}} \tag{21}$$

The correction for lower pressures has been a decisive factor to make the numerical results closer to the experimental data. This correction was not performed in previous results (Sabir et al. (1995); Ameel et al. (1996); Yang and Chen (1991); Yang and Wood (1991); Grossman and Gommed (1997); García-Rivera et al. (2012)) that leads to an overestimation of the influence of the non-absorbables.

5. Results and Discussions

In this section are shown the experimental data and its comparison against the numerical results. Has been evaluated the influence of different air concentrations ($w_{air} = 1{,}98\,\% - 37{,}31\,\%$) in the absorber performance under different working conditions, varying the Re number ($Re = 85 - 145$).

The experimental data obtained in the first point of the above list were used for validating the numerical model described in section 3.

5.1. Baseline Test

Before starting any experimental test, the minimum quantity of air that experiment allows was established by means the following tests:

- Mass spectrometry measurements during an experimental performance of absorption unit. The experimental unit was previously purged to obtain a vacuum of enough quality. During the experiment, the purge pumps keep turned off. The results were: $w_{air} = 1{,}851\,\%$ ($N_2 = 1{,}481\,\%$,$O_2 = 0{,}326\,\%$, $Ar = 0{,}042\,\%$).

- The same experiment was performed, but the purge pumps keep turned on during the whole test. The results are: $w_{air} = 1{,}857\,\%$ ($N_2 = 1{,}367\,\%$, $O_2 = 0{,}458\,\%$, $Ar = 0{,}029\,\%$).

From the tests performed it can be concluded: i) there are not important air leakages in the experimental setup; ii) the vacuum pumps are not able to remove the air inside completely; iii) the different proportions of the gases between the cases with and without connecting the purge system indicates absorption of oxigen by the $LiBr$ solution Chau et al. (1993). The table 3 shows the nominal characteristics in which the baseline test were performed.

Geometry	
Outer Diameter Tube (m)	0.022
Inner Diameter Tube (m)	0.018
Length Tube (m)	1.0
Working Conditions (LiBr Aqueous solution)	
Inlet Re number	$Re \approx$ 80-120
Inlet temperature (° C)	Saturation conditions (T_{sat})
Inlet LiBr concentration ($\%LiBr$)	60,2
Absorption pressure (Pa)	1300
Working Conditions Coolant Side	
Inlet solution mass flow (kgs^{-1})	1,19
Inlet temperature (° C)	29,91

Cuadro 3: Geometry and working conditions for the reference case.

5.2. Influence of Non-Absorbable concentrations

Taking as a reference the baseline case in the above section, a parametric study has been performed to evaluate the percentage of reduction of the heat and mass transfer rates influenced by non-absorbables concentration. Starting from the minimum air concentration achievable in the experimental setup, ($w_{air} \approx 1{,}85\,\%$), atmospheric air is introduced in steps of different concentrations until a maximum value of $w_{air} \approx 63\,\%$.

The Fig. 5 depicts the experimental results for the mass absorbed for different Re numbers and different air concentrations. As expected, the higher is the air concentration the more is the reduction of the rate of absorption. Same behavior is observed in Fig. 6, where the energy input through the interface and heat load ($\dot{Q}_{abs}$) are represented.

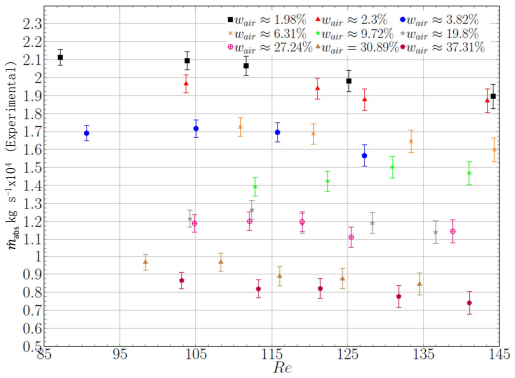

Figura 5: Experimental results of the mass absorbed ($\dot{m}_{abs}$) at different Re Number and under the influence of different air concentrations (w_{air})

The table 4 summarizes the average percentages of rate absorption reduction (R) at different air concentrations for mass and heat absorbed (Re≈120).

If the air concentration value is $w_{air} \approx 1{,}98\,\%$, it corresponds to a partial pressure of air of about $P_{air} \approx 16{,}2$ Pa if the total pressure value is $P_t = 1300$ Pa. The maximum value of $w_{air} \approx 37{,}31\,\%$ corresponds to a air partial pressure of about $P_{air} \approx 351{,}09$ Pa. At this point the percentage of reduction is near to 60 %. As expected, absorption performance degrades as air concentration increases.

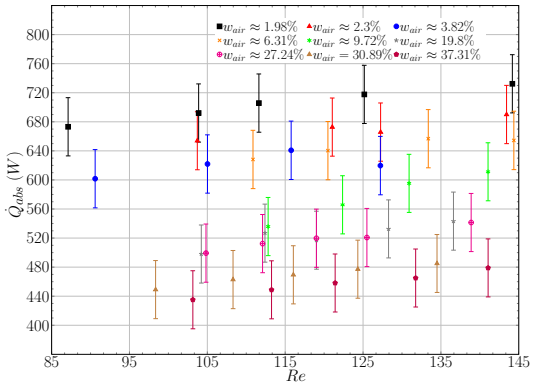

Figura 6: Experimental results of the heat load ($\dot{Q}_{abs}$) at different Re Number and under the influence of different air concentrations (w_{air}).

w_{air}	$\dot{m}_{abs}$ $(kg \cdot s^{-1})$	$(R)\,\%$	$\dot{Q}_{abs}$ (W)	$(R)\,\%$
1.98	1.98E-4	-	720.0	-
2.3	1.85E-4	6.5	691.3	4.0
3.82	1.62E-4	18.5	663.4	7.9
6.31	1.61E-4	18.6	655.4	9.0
9.72	1.33E-4	32.3	588.1	18.3
19.8	1.18E-4	40.7	544.2	24.4
27.24	1.18E-4	40.3	542.2	24.7
30.89	8.50E-5	57.1	485.8	32.5
37.31	7.72E-5	61.0	479.7	33.3

Cuadro 4: Comparison of average percentages of rate absorption reduction ($R\,\%$) for heat and mass absorbed at different air concentrations

5.3. Comparison with other authors

In this subsection, a comparison with results by other researchers has been performed. The selected bibliography is as follows: Yang (1987), Kim and Lee (2003) and Kim et al. (1995). In order to make the data comparable, the experimental results for the mass transfer have been adimensionalized using two different procedures.

First, it was used a similar procedure as Kim and Lee (2003) for the data reduction of the calculation of Sh values, in this case based on the logarithmic density difference of water species in solution between the vapor-liquid interface and the falling film bulk. For the points of our experiment and

the experiments of Yang (1987), the Sh calculation is based in logarithmic concentration differences of water species in solution between the vapor-liquid interface and the falling film bulk:

$$\Delta c = \frac{(c_{H2O,i,in} - c_{H2O,b,in}) - (c_{H2O,i,out} - c_{H2O,b,out})}{ln((c_{H2O,i,in} - c_{H2O,b,in})/(c_{H2O,i,out} - c_{H2O,b,out}))} \tag{22}$$

It should be noted that the concentrations at the bulk conditions are directly measured from the densimeters, but the concentrations at the interface are calculated at equilibrium conditions at interface, taking into account the partial vapour pressure of water at the absorber. The interface conditions are estimated by assuming heat and mass transfer analogy near the interface (see Yuksel and Schlunder (1987)):

$$\left[\frac{1 - X_b}{1 - X_{if}}\right]^{\frac{c_{pH_2O}/cp_s}{Le^{1-n}}} = \frac{c_{pH_2O}}{\Delta h_{abs}}(T_{if} - T_b) + 1 \tag{23}$$

Then, the mass transfer coefficient (β) an Sh number were calculated as follows:

$$\beta = \frac{\dot{m}_{abs}}{\rho A \Delta c} \tag{24}$$

$$Sh = \frac{\beta \delta}{D_l} \tag{25}$$

Figure 7 depicts the Sh number comparison for different air concentration values between our data and Yang (1987)Kim and Lee (2003). The Sh values decrease as the air concentration augmented. There is a reasonable agreement with the results, being the data of Yang (1987) more dispersed and separated

from the rest. The main reason of the separation is the use of aqueous LiCl solution, that gives results of the characteristic lenght ($(\nu^2/g)^{1/3}$) with a value about twice in comparison with aqueous LiBr. Hovewer, the results are quite consistent with the ones reported in this work.

A second comparison of Sh values has been performed following the data reduction procedure of Kim et al. (1995). In this case the concentration difference is calculated according to this expression:

$$\Delta c = ((p_{H2O,i,in} - p_{H2O,b,in})/2 + (p_{H2O,i,out} - p_{H2O,b,out})/2)\,\frac{\partial c}{\partial P} \tag{26}$$

A simple difference expression for calculating the mass transfer potential has been adopted. If offers similar results to the logarithmic difference, and allows to capture extra points due to that in our experiments the inlet conditions were very close to equilibrium.

Figure 8 depicts the comparison between our data against Yang (1987) Kim et al. (1995). Reasonable agreement is also found between data, being the data of Yang (1987) more dispersed and in general separated from the rest due to the question of the characteristic lenght.

Concerning heat transfer, the Nu values have been calculated using an energy balance in the falling film heat exchanger:

$$\dot{Q} = \dot{m}_c cp_c(T_{c,out} - T_{c,in}) = UA\Delta T \tag{27}$$

In the above expression, the temperature difference has been calculated according the logarithmic temperature difference:

$$\Delta T = \frac{(T_{c,in} - T_{s,in}) - (T_{c,out} - T_{s,out})}{ln((T_{c,in} - T_{s,in})/(T_{c,out} - T_{s,out}))} \tag{28}$$

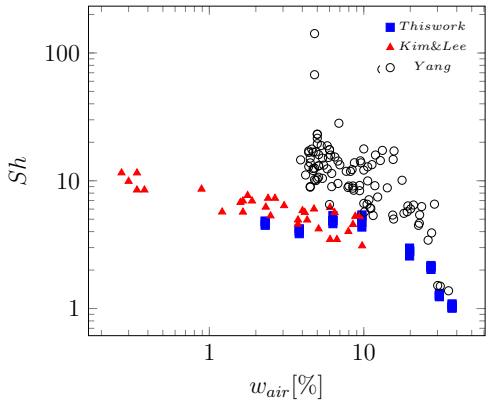

Figura 7: Comparison of experimental Sh number at different air concentrations w_{air}, according reduction procedure of Kim and Lee (2003)

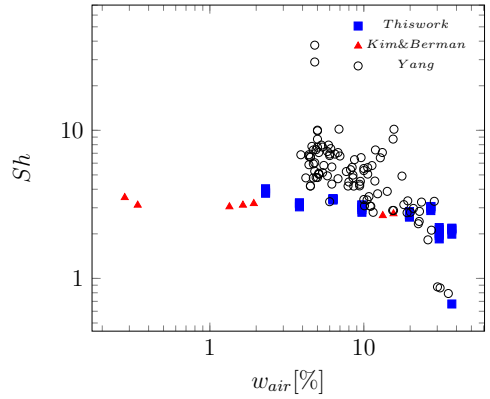

Figura 8: Comparison of experimental Sh number at different air concentrations w_{air}, according reduction procedure of Kim et al. (1995)

Finally, the falling film heat transfer coefficient is calculated taking into account the different heat transfer resistances:

$$\frac{1}{\alpha_f A_f} = (\frac{1}{UA} - \frac{ln(d_f/d_c)}{2\pi\lambda_{tube}L} - \frac{1}{\alpha_c A_c}) \tag{29}$$

Figure 9 depicts the Nu number variation at different air concentration values. As in the case of mass transfer, the results of the present research have a good matching with Kim et al. (1995), but data of Yang (1987) are more dispersed and separated. This behavior is due to, by one hand, the uncertainty in calculating the heat transfer in coolant side, because the author does not report the inner diameter accurately. On the other hand, another influencing factor is that Yang (1987) used $LiCl$ as working fluid, and this fact leads to important differences in the characteristic lenght. Moreover, it can be observed that in the data collected in this work the effect of the non-absorbables is slighty less important with respect Kim and Lee (2003) data.

5.4. Experimental Validation of the numerical model

In this section are compared the experimental data that were showed in section 5.2 against the numerical results of the mathematical model presented in section 3. An uncertainty analysis was conducted to determine the maximum error in experimental data, for further details see García-Rivera et al. (2016).

The Fig. 10 shows the comparison of the mass absorbed ($\dot{m}_{abs}$) between numerical results and experimental data results at different Re numbers ($Re = 85 \div 145$) and different air concentrations ($w_{air} = 1{,}98 \div 37{,}31\,\%$). The maximum error computed in uncertainty analysis is 8,6 %. Most of the points are within the range of error. The experimental data compared against mathematical model shows the following discrepancies: maximum 17,2 %, minimum 3,71 % and average 5,69 %.

The Fig. 11 shows comparison of the heat load ($\dot{Q}_{abs}$) between numerical and experimental results at different Re numbers ($Re = 85 \div 145$) and different air concentrations ($w_{air} = 1{,}98 \div 37{,}31\,\%$). The maximum error computed in the uncertainty analysis was 9 %. The experimental data compared

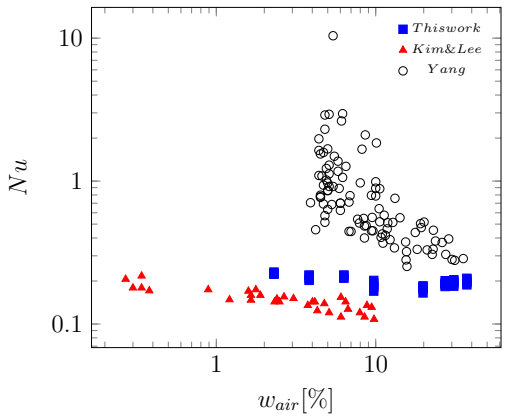

Figura 9: Comparison of experimental Nu number at different air concentrations w_{air}

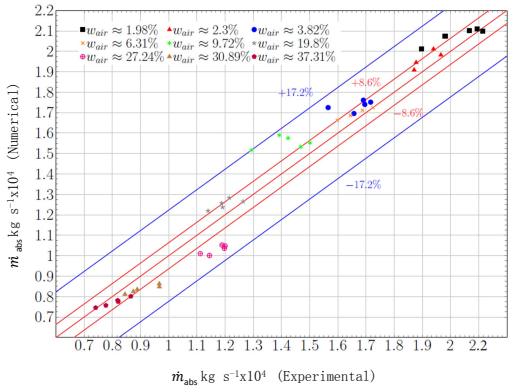

Figura 10: Comparison of the mass absorbed ($\dot{m}_{abs}$) between numerical and experimental results at different Re numbers ($Re = 85 \div 145$) and different air concentrations ($w_{air} = 1{,}98 \div 37{,}31\,\%$).

against the mathematical model shows the following discrepancies: maximum 17,5 %, minimum 2,53 % and average 7,8 %.

6. Conclusions

The influence of non-absorbable gases has been studied experimentally, with the help of mass spectrometry technique, able the quantify of non-absorbable gases in the experimental unit. Moreover, it has been developed a model for a vertical absorber based on Navier-Stokes equations together with energy and mass species conservation equations to consider the influence of non-absorbable in falling film absorption. Separated treatment has been considered for the liquid and vapor phases, with similar simplifications following boundary layer hipotheses. Wavy profiles are implemented together with falling film formulation using the Free Surface Deflection Equation.

The principal conclusions of each one:

1. As expected, the higher is the value of w_{air}, the lower is the performance of the absorber. The range of evaluation is $w_{air} = 1{,}98\,\%$ as minimum and $w_{air} = 37{,}31\,\%$ as maximum value. The maximum reduction in the heat and mass transfer rates of absorption are 66,06 % and 59,40 % respectively.

2. Comparing this results against other authors there is a reasonable agreement in terms of of Nu and Sh numbers, especially with Kim et al. (1995) and Kim and Lee (2003). Results of Yang (1987) offers more dispersion, due mainly to these experimental data has been obtained with smaller temperature differences, making the uncertainties in the measurements very important.

3. The experimental validation of the mathematical model presented show an acceptable agreement with the experimental results. The maximum, minimum and average discrepancies are as follows: i) mass absorbed $\dot{m}_{abs}$, maximum 17,2 %, minimum 3,71 % and average 5,69 %; ii) $\dot{Q}_{abs}$, maximum 17,50 %, minimum 2,53 % and average 7,80 %. Theerefore, the mathematical model and its numerical implementation are a simple but powerful tool for the design/prediction of vertical falling film absorbers.

7. Acknowledgments

This research has been financed and supported by the Spanish Government through the project "Modelización multiescala y simulación numérica directa de flujos multifásicos gas líquido en burbujas, películas y esprays (Ref. ENE2015-70672-P)" and by the EIT through KIC Innoenergy project "Energy storage as necessary part of energy balanced building and districts".

ApéndiceA. Experimental Data

This appendix contains the experimental data that allows to perform the energy and mass balances. The table A.5 shows the inlet/outlet conditions and the mass absorbed $\dot{m}_{abs}$ in the falling film side at different air concentrations w_{air}. The table A.6 shows the inlet/outlet conditions and the heat rate removed $\dot{Q}_{abs}$ in the coolant side at different air concentrations w_{air}.

Ablanque, N., Oliet, C., Rigola, J., Segarra, C. D., Oliva, A., 2015. Numerical Simulation of Non-adiabatic Capillary Tubes. Special Emphasis on the Near-saturation Zone. International Journal of Refrigeration 55 (1), 153–167.

Ameel, T. A., Habib, H. M., Wood, B. D., 1996. Effects of Nonabsorbable Gas on Interfacial Heat and Mass Transfer for the Entrance Region of a Falling Film Absorber. Journal of Solar Energy Engineering 118 (1996), 45–49.

Bennett, C. O., Myers, J. E., 1975. Momentum, Heat, and Mass Transfer. McGraw-Hill.

Bird, R. B., Stewart, E. E., Lightfoot, E. N., 1960. Transport Phenomena. John Wiley and Sons Inc.

Chau, S., Wood, B. D., Berman, N. S., Kim, K. J., 1993. Solubility of oxygen in aqueous lithium bromide using electrochemical technique. International Communications in Heat and Mass Transfer 20, 751–760.

Dietze, G. F., 2010. Flow Separation in Falling Films. Ph.D. thesis, Von der Fakultät fur Machinenwesen der Rheinisch-Westfälischen Technischen Hochschule Aachen.

	Inlet conditions			Outlet conditions		Results
Re	$\dot{m}_{l,in}$ $(\frac{kg}{s})$	$T_{l,in}$ $(\cdot C)$	$c_{l,in}$	$T_{l,out}$ $(\cdot C)$	$c_{l,out}$	$\dot{m}_{abs}$ $(\frac{kg}{s})$
	$w_{air} = 2{,}3\,\%$					
124	1.105e-02	49.51	6.006e-01	41.40	5.907e-01	1.85E-04
110	9.891e-03	49.11	6.009e-01	41.23	5.896e-01	1.90E-04
104	9.448e-03	49.07	6.014e-01	41.40	5.891e-01	1.97E-04
89	8.194e-03	48.59	6.018e-01	40.81	5.875e-01	1.97E-04
	$w_{air} = 3{,}82\,\%$					
126.5	1.12e-02	49.42	6.007e-01	40.97	5.920e-01	1.66E-04
110	9.857e-03	49.33	6.011e-01	40.75	5.916e-01	1.59E-04
100	9.030e-03	49.44	6.019e-01	40.29	5.908e-01	1.71E-04
91	8.171e-03	49.82	6.024e-01	40.12	5.900e-01	1.71E-04
	$w_{air} = 6{,}31\,\%$					
125	1.100e-02	49.9	6.003e-01	40.89	5.917e-01	1.61E-04
115	1.023e-02	49.61	6.007e-01	40.56	5.909e-01	1.69E-04
104	9.308e-03	49.34	6.008e-01	40.30	5.900e-01	1.71E-04
96	8.546e-03	49.71	6.001e-01	40.11	5.892e-01	1.72E-04
	$w_{air} = 9{,}72\,\%$					
129	1.126e-02	49.50	5.988e-01	40.37	5.918e-01	1.33E-04
122	1.071e-02	49.40	5.990e-01	40.21	5.908e-01	1.49E-04
113	9.961e-03	49.45	5.991e-01	40.12	5.903e-01	1.49E-04
106	9.933e-03	49.29	5.993e-01	40.12	5.902e-01	1.44E-04
98	8.650e-03	49.17	5.995e-01	39.99	5.899e-01	1.41E-04
	$w_{air} = 19{,}8\,\%$					
118	1.0403e-02	49.61	5.997e-01	38.71	5.930e-01	1.18E-04
113	9.9950e-03	49.51	6.000e-01	38.60	5.926e-01	1.23E-04
102	9.1420e-03	49.41	6.003e-01	38.57	5.924e-01	1.21E-04
99	8.7750e-03	49.80	6.006e-01	38.34	5.918e-01	1.29E-04
90	7.9890e-03	49.73	6.007e-01	38.48	5.916e-01	1.23E-04
	$w_{air} = 27{,}24\,\%$					
120	1.0603e-02	49.26	5.993e-01	37.80	5.927e-01	1.18E-04
108	9.5510e-03	49.44	5.994e-01	37.44	5.922e-01	1.16E-04
97	8.5510e-03	49.51	5.996e-01	37.44	5.912e-01	1.21E-04
90	7.9870e-03	49.57	5.997e-01	37.22	5.907e-01	1.23E-04
	$w_{air} = 30{,}89\,\%$					
116	1.0252e-02	49.36	5.992e-01	35.74	5.942e-01	8.50E-05
107	9.4470e-03	49.58	5.994e-01	35.59	5.937e-01	9.00E-05
100	8.7900e-03	49.80	5.995e-01	35.51	5.933e-01	9.20E-05
94	8.1910e-03	50.08	5.997e-01	35.32	5.927e-01	9.70E-05
85	7.4350e-03	50.11	6.000e-01	35.20	5.920e-01	1.00E-04
	$w_{air} = 37{,}31\,\%$					
122	1.075e-02	49.33	5.993e-01	35.38	5.950e-01	7.77E-05
114	1.005e-02	49.31	5.993e-01	35.12	5.946e-01	8.10E-05
105	9.204e-03	49.71	5.995e-01	35.02	5.940e-01	8.60E-05
98	8.503e-03	50.13	5.996e-01	34.69	5.937e-01	8.50E-05
89	7.782e-03	50.21	5.998e-01	34.58	5.931e-01	8.70E-05

Cuadro A.5: Experimental data in the falling film side at different Re numbers and different air concentrations w_{air}.

Re	Inlet conditions		Outlet conditions	Results
	$\dot{m}_{c,in}$ $(\frac{kg}{s})$	$T_{c,in}$ $(\cdot C)$	$T_{c,out}$ $(\cdot C)$	$\dot{Q}_{abs}$ (W)
	$w_{air} = 2{,}3\,\%$			
10872	0.1196	29.90	31.28	6.91E+02
10862	0.1195	29.90	31.24	6.67E+02
10846	0.1193	29.90	31.25	6.74E+02
10816	0.1190	29.90	31.22	6.55E+02
	$w_{air} = 3{,}82\,\%$			
10890	0.1199	29.90	31.23	6.63E+02
10881	0.1199	29.91	31.14	6.21E+02
10888	0.1198	29.91	31.19	6.42E+02
10861	0.1195	29.91	31.15	6.23E+02
	$w_{air} = 6{,}3182\,\%$			
10892	0.1199	29.90	31.21	6.55E+02
10855	0.1195	29.90	31.22	6.58E+02
10854	0.1195	29.90	31.18	6.41E+02
10865	0.1197	29.90	31.16	6.29E+02
	$w_{air} = 9{,}72\,\%$			
10803	0.1190	29.92	31.10	5.88E+02
10812	0.1191	29.92	31.15	6.12E+02
10820	0.1192	29.92	31.11	5.96E+02
10827	0.1194	29.92	31.05	5.67E+02
10823	0.1194	29.92	30.99	5.37E+02
	$w_{air} = 19{,}8\,\%$			
10810	0.1192	29.92	31.01	5.44E+02
10795	0.1191	29.92	30.99	5.33E+02
10791	0.1191	29.92	30.96	5.18E+02
10797	0.1191	29.92	30.98	5.28E+02
10795	0.1192	29.92	30.92	4.99E+02
	$w_{air} = 27{,}24\,\%$			
10817	0.1193	29.92	31.01	5.42E+02
10818	0.1194	29.92	30.96	5.22E+02
10824	0.1195	29.92	30.96	5.21E+02
10825	0.1194	29.92	30.95	5.13E+02
10819	0.1195	29.92	30.92	5.00E+02
	$w_{air} = 30{,}89\,\%$			
10766	0.1189	29.92	30.89	4.86E+02
10789	0.1192	29.92	30.88	4.78E+02
10803	0.1193	29.92	30.86	4.70E+02
10811	0.1194	29.92	30.85	4.64E+02
10775	0.1191	29.92	30.82	4.49E+02
	$w_{air} = 37{,}31\,\%$			
10778	0.1191	29.91	30.88	4.80E+02
10786	0.1192	29.92	30.85	4.66E+02
10760	0.1189	29.92	30.84	4.58E+02
10774	0.1191	29.92	30.82	4.50E+02
10779	0.1192	29.92	30.79	4.36E+02

Cuadro A.6: Experimental data in the coolant side at different Re numbers and different air concentrations w_{air}.

García-Rivera, E., Castro, J., Farnós, J., Oliva, A., 2012. Modelling of Absorption of H2O Vapor in Falling Film of LiBr Aqueous Solution in Vertical Tubes with Presence of Non-Condensables. In: Proceedings of the 10th IIR Gustav Lorentzen Natural Working Fluids Conference. pp. 263–270.

García-Rivera, E., Castro, J., Farnós, J., Oliva, A., 2016. Numerical and Experimental Investigation of a LiBr Falling Film Vertical Absorber Considering Wave Regimes and in Presence of Mist Flow. International Journal of Thermal Sciences 109 (1), 342–361.

Gnielinski, V., 1976. New equations for heat and mass transfer in turbulent pipe and channel flow. International Chemical Engineering 16 (2), 359–368.

Grossman, G., Gommed, K., 1997. Heat and mass transfer in film absorption in the presence of non-absorbable gases. International Journal of Heat and Mass Transfer 40 (15), 3595–3606.

Hirshburg, R. I., 1980. Laminar Film FLow Phenomena, Theory and Application to the Two-Phase Closed Thermosyphon. Ph.D. thesis, Arizona State University.

Hirshburg, R. I., Florschuetz, L. W., 1982a. Laminar Wavy-Film Flow: Part I, Hydrodynamic Analysis. ASME J. Heat Transfer 104 (1), 452–458.

Hirshburg, R. I., Florschuetz, L. W., 1982b. Laminar Wavy-Film Flow: Part II, Condensation and Evaporation. ASME J. Heat Transfer 104 (1), 459–464.

Kim, B., Lee, C., 2003. Non-Absorbable Gas Effects on Heat and Mass Transfer in Falling Film Absorption. Journal of Mechanical Science and Technology 17 (4), 581–589.

Kim, K. J., Ameel, T. A., Wood, B. D., 1996. Performance Evaluations of LiCl and LiBr Absorber Design Applications in the Open Cycle Absorption Refrigeration System. Journal of Solar Energy Engineering 119 (1997), 165–173.

Kim, K. J., Berman, N. S., Chau, D. S. C., Wood, B. D., 1995. Absorption of Water vapour into falling films of aqueous lithium bromide. International Journal of Refrigeration 18 (7), 486–494.

Medrano, M., Bourouis, M., Perez-Blanco, H., Coronas, A., 2003. A simple model for falling film absorption on vertical tubes in the presence of non-absorbables. Industrial and Engineering Chemical Fundamentals 26 (2003), 108–116.

Ravigururajan, T., Bergles, A., 1996. Development and Verification of General Correlations for Pressure Drop and Heat Transfer in Singel-Phase Turbulent Flow in Enhanced Tubes. Exp. Thermal and Fluid Science 13 (1), 55–70.

Sabir, H., Suen, K. O., Vinnicombe, G. A., 1995. Investigation of effects of wave motion on the performance of a falling film absorber. International Journal of Heat and Mass Transfer 39 (12), 2463–2477.

Welty, J. R., Wicks, C. E., Wilson, R. E., Rorrer, G. L., 2008. Fundamentals of momentum, Heat and Mass Transfer. Willey.

Yang, R., 1987. Heat and Mass Transfer in Laminar Wavy Film Absorption with the Presence of Non-Absorbable Gases. Ph.D. thesis, Arizona State University.

Yang, R., Chen, J. H., 1991. A Numerical Solution of the non-absorbable effects on the falling liquid film absorption. Wärme und Stoffübertragung 26 (1991), 219–223.

Yang, R., Jou, D., 1993. Heat and Mass Transfer on Wavy Film Absorption Process. Solar Energy 71 (3), 533–538.

Yang, R., Jou, T. M., 1998. Non-absorbable gas effect on the wavy film absorption process. International Journal of Heat and Mass Transfer 41 (22), 3657–3668.

Yang, R., Wood, D., 1991. A Numerical Solution of the Wavy Motion on a Falling Liquid Film. Solar Energy 69 (1), 723–728.

Yuksel, M., Schlunder, E., 1987. Heat and Mass Transfer in Non-isothermal Absorption of Gases in Falling Liquid Films. part i: Experimental Determination of Heat and Mass Transfer Coefficients. Chemical Engineering and Processing: Process Intensification 22 (4), 193–202.

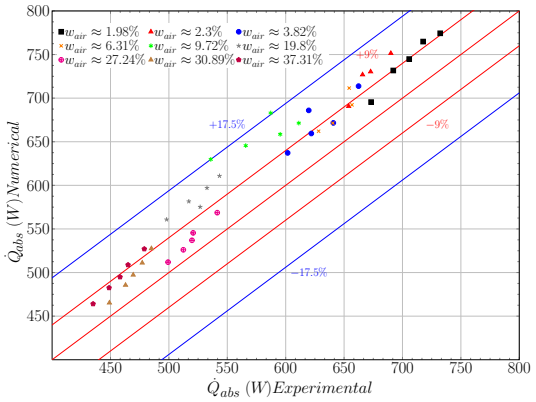

Figura 11: Comparison of the heat ($\dot{Q}_{abs}$) load between numerical and experimental results at different Re numbers ($Re = 85 \div 145$) and different air concentrations ($w_{air} = 1{,}98 \div 37{,}31\,\%$).